Creep-Fatigue Crack Growth Behavior of a Structure with Crack Like Defects at the Welds

Hyeong-Yeon Lee*, Seok-Hoon Kim, Jae-Han Lee and Byung-Ho Kim
Mechanical Engineering Division, Korea Atomic Energy Research Institute, 150 Dukjin-dong, Yuseong-gu, Daejeon 305-353, Korea

A study on a creep-fatigue crack growth behavior has been carried out for a cylindrical structure with weldments by using a structural test and an evaluation according to the assessment procedures. The creep-fatigue crack growth behavior following the creep-fatigue crack initiation has been assessed by using the French A16 procedure and the conservatism for the present structural test has been examined. The structural specimen is a welded cylindrical shell made of 316 L stainless steel (SS) for one half of the cylinder and 304 SS for the other half. In the creep-fatigue test, the hold time under a tensile load which produces the primary nominal stress of 45 MPa was one hour at 600℃ and creep-fatigue loads of 600 cycles were applied. The evaluation results for the creep-fatigue crack propagation were compared with those of the observed images from the structural test. The assessment results for the creep-fatigue crack behavior according to the French A16 procedure showed that the A16 is overly conservative for the creep-fatigue crack propagation in the present case with a short hold time of one hour.

Key Words : Creep-Fatigue, Crack Growth, Weld, Stress Intensity Factor

1. Introduction

An assessment of a creep-fatigue crack initiation and growth is one of the key factors in the design and evaluation of a high temperature structure such as a Liquid Metal Reactor (LMR), KALIMER (Korea Advanced LIquid MEtal Reactor) (Hahn et al., 2004) subjected to thermal cycles at a creep regime. The design of a reactor system and the components under a creep-fatigue load can be carried out by using high temperature design codes such as ASME-NH (ASME, 2004), RCC-MR (RCC-MR, 2002), and DDS (DDS, 1998), which provide the linear damage summation rule for an evaluation of the creep-fatigue damage.

* Corresponding Author,
E-mail : hylee@kaeri.re.kr
TEL : +82-42-868-2956; **FAX** : +82-42-861-7697
Mechanical Engineering Division, Korea Atomic Energy Research Institute, 150 Dukjin-dong, Yuseong-gu, Daejeon 305-353, Korea. (Manuscript **Received** May 12, 2006; **Revised** September 25, 2006)

For a defect free structure operating at a high temperature, the codes provide the procedures of an elastic and an inelastic analysis for the creep-fatigue damage limits. However, the design codes do not provide the rules for the assessment of a structure with defects. The A16 (Subsection, 2002) guide which has been included in edition 2002 of the RCC-MR provides the procedure for a creep-fatigue assessment for a structure with a defect. In the present study, the A16 procedure was employed for an evaluation of the creep-fatigue crack growth for a cylindrical shell with defects. The A16 procedure for the creep-fatigue crack initiation for the present structural model was shown to be reasonably conservative when compared to the observation images from the structural tests (Lee et al., 2006a).

The A16 procedure provides the creep-fatigue assessment procedures for a structure with defects based on the fracture mechanics parameters K_I, J, C^*. Researches on quantifying the conservatism have mainly been carried out at the level of material specimens (Drubay et al., 2003 ; Chellapandy

et al., 2005) rather than structural specimens in terms of the observed images. In this study, the conservatism of the A16 procedure for a creep-fatigue crack propagation of the present cylindrical shell specimen with weldments at the base metal and the weld metal has been quantified. The creep-fatigue load was applied 600 times with a tensile hold time of one hour and the aspects of the creep-fatigue crack behavior were observed periodically with a portable optical microscope at every 100^{th} cycle non-destructively. The assessment results according to the A16 procedure were compared with the observed images.

2. Structural Test

2.1 Structural specimen

The test facility used for the present creep-fatigue structural test is shown in Fig. 1. It is composed of a hydraulic actuator of a 1 MN capacity and a high frequency induction heating unit with a capacity of 50 kW (Kim et al., 2005). The test specimen with 6 turns of an inductance coil is shown in Figs. 1(b) and 3.

The configuration of the liquid metal reactor, KALIMER-600 which is the target structure for an application of the present study is shown in Fig. 2. The structural specimen shown in Figs. 1 (b) and 3 has the dimensions of a 600 mm diameter, a 500 mm height and a 7 mm thickness. Similar type of cylindrical shell specimens with weldments were used for the thermal ratcheting structural tests (Lee et al., 2003 ; 2004).

The specimen is a welded cylindrical shell with one half a 304 stainless steel (SS) shell and the other half a 316L SS one as shown in Fig. 3. The two plates of the 304 and 316L materials were welded as shown in Fig. 3(b) with the welding methods of a SMAW (Shielded Metal Arc Welding) and a GTAW (Gas Tungsten Arc Welding). The behavior of the two welding methods under a creep-fatigue load is examined at similar and dissimilar metal welds.

There are similar metal welds between the 304 and 304, and between the 316L and 316L while there is a sort of a dissimilar metal weld between the 304 and 316L at the mid-interface. Although 304 and 316L are both austenitic stainless steel, the creep behavior and creep rupture strength of the two materials at 600℃ are quite different,

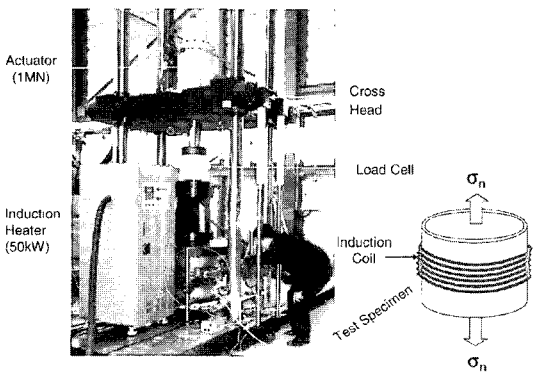

Fig. 1 Creep-fatigue test facility

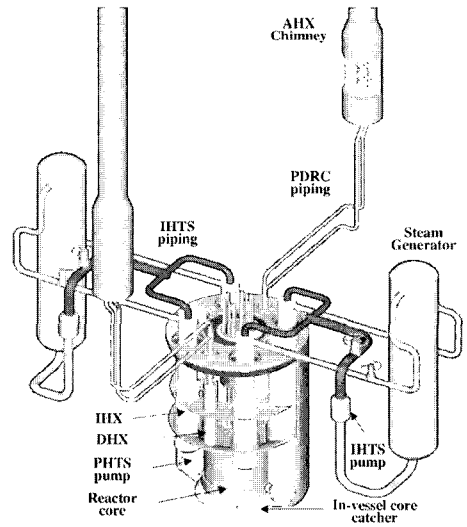

Fig. 2 Liquid metal reactor, KALIMER-600

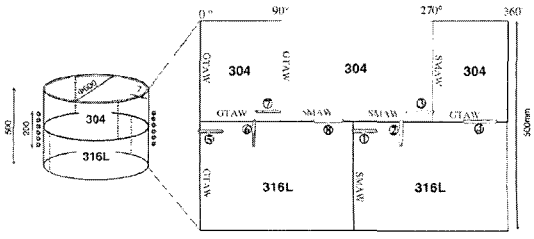

Fig. 3 Creep-fatigue test model and its development figure

which is why the welds between the two materials are here referred to dissimilar metal welds in this paper.

Eight crack-like defects were machined by an electrical discharge machining (EDM) as shown in Fig. 3(b). In Fig. 3(b), each defect has the dimensions of a height of 0.3 mm and a length of 40 mm. Defect numbers (#) 1 and #5 are the surface defects with a half penetration of 3.5 mm (thickness is 7 mm) uniformly along the circumferential direction from the inside surface and all the other defects are the through-wall type. Defect numbers of #4 and #8 are machined along the mid weld interface line between the 304 and 316L shell. The tips of each defect are located either at the weld metal or at the base metal, and no tips were located at the heat affected zone (HAZ). The specimen was welded with two passes and the welding conditions of a current of 110~120(A), voltage of 26~30(V), heat input of 2.0~2.5(KJ/mm), and a speed of 80~150(mm/min) for the two welding methods. The filler metal of ER316L SS which has a superior creep rupture strength to 304SS was used as a weld metal for all the welded joints.

An inspection by using the X-ray diffraction method was carried out to see if there were any internal weld defects along all the weld lines of the specimen. Tiny internal weld defects were found at a few locations but the 8 defects were machined far enough away from the internal defects so that their effects would be negligible.

2.2 Load conditions

The specimen of Fig. 3(a) is subject to a thermal cycling with a steady mechanical load. The specimen is heated up to 600℃ and a tensile hold time of one hour has been applied under a load control condition as shown in Fig. 4. The inductance coil covers the mid 200 mm part of the specimen as shown in Figs. 1(b) and Fig. 3(a). The temperature profiles measured along the axial direction are shown in Fig. 5 and they were used in the thermal analysis.

As shown in Fig. 4, it took about 9 minutes to reach 600℃ from 70℃ and 21 minutes to cool down again to 70℃ at a mid part of the specimen.

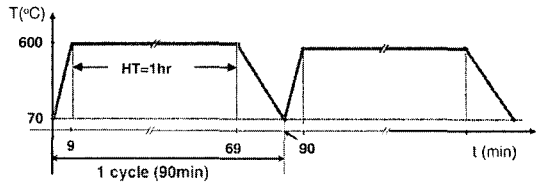

Fig. 4 Thermal load conditions

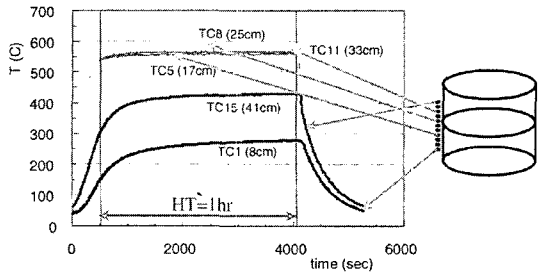

Fig. 5 Measured temperature data on the outer surface of the specimen

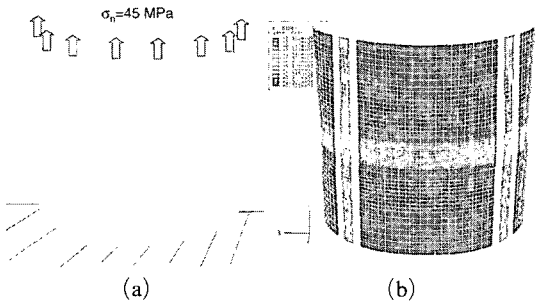

Fig. 6 Load and boundary condition of FE model, and principal stress distribution (scale factor : 481)

Mechanical load of 60 tons was been applied in the axial direction and the axial nominal stress was 45 MPa as shown in Fig. 6(a). So, one cycle with one hour of a tensile hold time was about 90 minutes. Totally 600 creep-fatigue load cycles were applied and it took about 6 months to carry out the structural test and observation of the damage and crack growth.

3. Assessment of the Creep-Fatigue Crack Behavior

3.1 Finite element modeling

A three dimensional half symmetric model with 4 defects was used for the ABAQUS (2005) finite

element analysis as shown in Fig. 6(a). A total of 53,760 8-node linear brick elements and 73,228 nodes were used. The element size in front of the tip in horizontal axis direction is selected as 0.24 mm so that the Gaussian point will be located exactly at 0.05 mm (=50 μm) from the notch tip. The height of each notch having a root radius of 0.15 mm is 0.3 mm and the semi-circular shaped notch was modeled with four elements in the vertical direction. The size of the tip element (parallelogram shape) is 0.24(mm) ×0.015(mm). Thermal loads shown in Fig. 5 and a mechanical stress of 45 MPa were applied, and the bottom surface was fixed as a boundary condition as shown in Fig. 6(a). Among the 4 crack-like defects in the half symmetric model, there is one surface defect (#1), one vertical through wall defect (#2) and the others (#3, #4) are horizontal through wall defects. The distribution of Mises stresses are shown in Fig. 6(b) (deformation scale factor is 300).

Here, the finite element analysis results were used in the evaluation according to ASME-NH and are described in section 3.3. In A16 guide, formula type compendia on the assessment on a creep-fatigue crack propagation for a tube, plate, bar, elbow, piping tee and nozzle are provided for the mechanical and thermal loads.

The effect of a weld residual stresses for the typically simple weld geometries can be assessed by using the assessment procedures of R6 (British Energy, 2001) or BS7910 (British Standard, 2000; Lee et al., 2006b; 2006c) but in general the residual stresses at a high temperature tend to relax and they are known to initiate a crack but they do not contribute a crack growth (Lee et al., 2006d).

3.2 Assessment of creep-fatigue crack growth according to the A16 procedure

In the French RCC-MR code (RCC-MR, 2002; A16, 2002), the geometrical discontinuities are assimilated with cracks for a creep-fatigue estimation based on an simplified elastic analysis. The creep-fatigue crack initiation of the A16 procedure is based on the sigma-d (σ_d) method where the distance 'd' is specified as '0.05 mm' for austenitic stainless steels (Drubay, 2003). The assessment on the creep-fatigue crack initiation has been carried out in a previous study (Lee et al., 2006a). It has been shown that the first creep-fatigue crack initiation occurred at defect #3 of Fig. 3 and the assessment results for a creep-fatigue crack initiation were shown to be reasonably conservative when compared to those of the test results.

The amount of creep-fatigue crack growth in the A16 guide is determined by linearly adding the fatigue crack growth and creep crack growth. The creep crack growth rate is derived from a C^* evaluation based on the reference stress concept and the da/dt-C^* material curve in this paper. A creep-fatigue crack propagation should be evaluated if the number of cycles for the creep-fatigue crack initiation is less than the actual load cycles.

3.2.1 Calculation of the fatigue crack growth (δa_f)

The maximum effective stress intensity factor (SIF) range should be determined to calculate the updated size of the defect due to a fatigue load. The fatigue crack growth is estimated from the Paris law with a SIF range of ΔK_{eff} derived from a simplified cyclic J-integral range of ΔJ during a cycle based on the reference stress concept.

$$\Delta K_{eff} = q\sqrt{E^* \Delta J} \tag{1}$$

where q is the closure ($R<0$) and mean stress ($R>0$) coefficient, E^* is E for the plane stress and $E/(1-v^2)$ for the plane strain, and R is the minimum to maximum load ratio. In the A16 guide, the SIF K_I for a circumferential defect is given by

$$K_I = (\sigma_m F_m + \sigma_b F_b + \sigma_{gb} F_{gb})\sqrt{\pi c} \tag{2}$$

where σ_m, σ_b and σ_{gb} are the membrane, bending and global bending stress, respectively. And F_m, F_b and F_{gb} are the influence coefficients and $2c$ is the length of the defect.

The J-integral in the A16 guide under a combined mechanical loading and a thermal gradient is

$$J_s = \left[\sqrt{J_{el}^{me}} + \frac{\sigma^{me+th}}{\sigma_{el}^{me+th}}\sqrt{J_{el}^{th}}\right]^2 \frac{E \cdot \varepsilon_{ref}^{me+th}}{\sigma_{ref}^{me+th}} \tag{3}$$

where J_{el}^{me} and J_{el}^{th} are an elastically calculated J-integral due to a mechanical load and thermal gradients ($J_{el}^{me}=(K_{eq}^{me})^2/E^*, J_{el}^{th}=(K_{eq}^{th})^2/E^*$; $E^*=E/(1-v^2)$ for plane strain, $E^*=E$ for plane stress), the reference stress and reference strain under a mechanical stress and thermal gradients (σ_{ref}^{me+th} & $\varepsilon_{ref}^{me+th}$) are shown in Fig. 7. In Fig. 7, the reference stress σ_{ref}^{me+th} and reference strain $\varepsilon_{ref}^{me+th}$ are determined by taking predetermined reference stresses due to mechanical and thermal stress (σ_{ref}^{me} and σ_{ref}^{th}) into account using the rational average tensile curve. The spring effect coefficient of r_{th} for the present circumferential throughwall defect problem is specified as zero in A16 guide. Then the calculated J-integral at defect #3 becomes $J_s=4.096$(N/mm) for the base metal of 304 SS, and $J_s=4.084$(N/mm) for the weld metal of ER316L.

The increment of a fatigue propagation for each cycle type i at a base metal of defect #3 is calculated from the following formula, which is com monly used for the base metal and the weld metal;

$$(\delta a_f)_i=C\cdot[(\Delta K_{eff})_i]^n \tag{4}$$

where $(\Delta K_{eff})_i$ is the effective SIF range for cycle type i. It should be noted that the coefficients $C=6\times10^{-8}$ and $n=3.3$(A3, 2003) are the same for 304 and 316L stainless steel. From Eq. (4) the fatigue crack growth rate for the base metal can be calculated by equation (5).

$$\frac{da}{dN_f}=0.00268[\text{mm/cycle}] \tag{5}$$

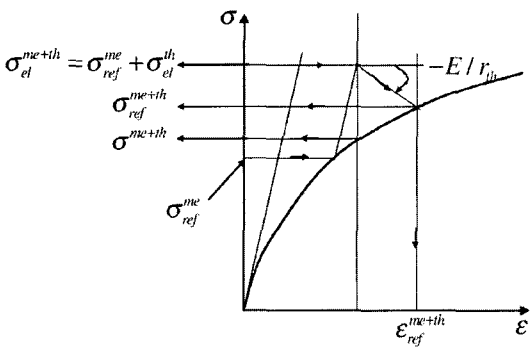

Fig. 7 The reference stress and strain in A16 guide

Then the increment of a fatigue crack growth for defect #3 at a base metal (304 SS) is given as Eq. (6).

$$(\delta a_f)_{i,base}=0.00268\,(\text{mm}) \tag{6}$$

The increment of a fatigue crack growth at the weld metal (ER316L) of defect #3 can be similarly calculated by taking the difference of the material properties such as the material tensile curves into account. In this case the increment for the weld metal was found to be slightly less than that of the base metal as shown in Eq. (7).

$$(\delta a_f)_{i,weld}=0.00225\,(\text{mm}) \tag{7}$$

3.2.2 Calculation of the creep crack growth (δa_c)

In the calculation of the creep crack growth (δa_c), the $C^*(t)$ should be determined during the hold time by taking into account the hold time and by using the creep crack propagation law.

The amount of a creep propagation during the hold time t_{mi} is calculated from the following formula;

$$C_s^*=\left[\sqrt{J_{el}^{me}}+\frac{\sigma^{me+th}}{\sigma_{el}^{me+th}}\sqrt{J_{el}^{th}}\right]^2\frac{E\cdot\dot{\varepsilon}_{ref}^{me+th}(t)}{\sigma_{ref}^{me+th}(t)} \tag{8}$$

$$(\delta a_c)_i=\int_{t_1}^{t_i+t_{mi}}A[C_i^*(t)]^q dt \tag{9}$$

where $\dot{\varepsilon}_{ref}^{me+th}(t)$ is the creep strain rate calculated for the stress $\sigma_{ref}^{me+th}(t)$ and $C_i^*(t)$ is the C^* integral whose formula is provided (A16, 2002)

$$\frac{da}{dt}=A(C^*)^q \tag{10}$$

where $A=8.05$, $q=0.81$ (A16, 2002), and t_i is a time to cycle type i and t_{mi} is a holding time. Here the C_s^* is calculated to be $C_s^*=9.267$(N/mm·hr) for the base metal and $C_s^*=4.048$(N/mm·hr) for the weld metal.

Thus the amount of creep crack growth per cycle for the base metal and weld metal is

$$(\delta a_c)_{i,base}=0.49\,(\text{mm}) \tag{11}$$

$$(\delta a_c)_{i,weld}=0.25\,(\text{mm}) \tag{12}$$

It is interesting to note that the increment of the creep crack growth for the weld metal is about

half of the base metal as shown in Eqs. (11) and (12). The differences of the two values are mainly judged to be caused by the differences of the creep properties between 304 (base metal) and 316L (weld metal). The strain rate term of $\dot{\varepsilon}_{ref}^{me+th}(t)$ in Eq. (8) for 316L is quite different from that for 314, which consequently can cause a big difference in creep crack growth increment as in Eqs. (11) and (12). Since the creep strength of 304 SS is weaker than 316L, the base metal part (304 SS) has been estimated to be weaker than the weld metal part (316L SS). RCC-MR employs the Bailey-Norton (Kraus, 1980) creep law for 316L and the Kraus creep law (Kraus, 1980) for 304SS.

It should be noted that the creep crack increments in Eqs. (11) and (12) are overly conservative for the present case of creep-fatigue loading with a short hold time like one-hour. Since the A16 procedure is intended to carry out a defect assessment for a component operating at high temperature with a long hold time like 10,000 hours (with total design life of 300,000 hrs), its assessment results may be quite different from the actual observation for the case with a short hold time like one hour. However, the procedure needs to be improved to assess more reasonably for the creep or creep-fatigue problem dominated by primary creep. The crack growth characteristics showing more damage at the base metal than at the weld metal are in agreement with the observed images, which is discussed in the next section. Based on the present assessment, it is concluded that the A16 procedure provides overly conservative results for a creep-fatigue creep crack growth problem in the case of a short hold time such as one-hour.

3.3 Applicability of ASME-NH code

ASME-NH code is the design guidelines for a defect free structure. However, the applicability of the ASME-NH to the notch tip of the crack-like defect was investigated in this study.

In order to evaluate the creep-fatigue damage according to ASME-NH, the equivalent stress concentration factor (SCF) should be determined with the effective primary stress (P), secondary stress (Q) and peak stress (F) by using the FE results. The calculated result is given in Eq. (9).

$$\text{equiv.SCF}=\frac{\text{effective(P+Q+F) (von Mises)}}{\text{effective(P+Q)}}=2.12 \tag{13}$$

At the notch tip element of defect #3, the calculated strains in Eq. (14) show that they are almost in a triaxial strain state which makes the deviatoric strain very small.

$$\begin{aligned}\varepsilon_{11}&=0.0111\\ \varepsilon_{22}&=0.0110\\ \varepsilon_{33}&=0.0116\end{aligned} \tag{14}$$

Thu the resulting equivalent strain in Eq. (15) (ASME, 2004) is calculated to be $\Delta\varepsilon_{equiv,i}=0.000146$, which is very small and consequently the creep and fatigue damage should be negligible.

$$\Delta\varepsilon_{equiv,i}=\frac{\sqrt{2}}{2(1+\nu^*)}\left[(\Delta\varepsilon_{x_i}-\Delta\varepsilon_{y_i})^2+(\Delta\varepsilon_{y_i}-\Delta\varepsilon_{z_i})^2+(\Delta\varepsilon_{z_i}-\Delta\varepsilon_{x_i})^2+\frac{3}{2}(\Delta\gamma^2_{xy_i}+\Delta\gamma^2_{yz_i}+\Delta\gamma^2_{zx_i})\right] \tag{15}$$

When the total strain range with Eq. (15) is calculated, the endurance limit and rupture time are determined as in Eq. (16)

$$\begin{aligned}N_d&\rightarrow\infty\\ T_d&=3\times10^5\end{aligned} \tag{16}$$

Then the creep-fatigue damage under the ASME-NH rule for the present case at the notch tip can be described as in Eq. (17) by summing the fatigue damage (A) and creep damage (W).

$$A+W=\frac{n}{\infty}+\frac{t}{3\times10^5} \tag{17}$$

This means that ASME-NH is not appropriate for an evaluation of the creep-fatigue damage near the notch tip due to the tri-axial strain state, which can be seen from the observed images.

4. Observation of a Creep-Fatigue Damage

The creep-fatigue damage aspects of the test model at the notch tips have been inspected with an optical microscope intermittently after every 100^{th} cycle in a non-destructive way. Various creep-fatigue damage aspects at or near the notch tips

were investigated during the inspection. The behavior of the defect geometries (vertical and horizontal defects), and that of the two welding methods (GTAW and SMAW) under a creep-fatigue load have been examined.

The images of horizontal defect #3 showed that it was the most damaged among the eight defects examined. The observed images of Figs. 8 and 9 for defect #3 showed that the crack is propagated as much as 0.39 mm for the weld metal (SMAW) and 0.79 mm for the base metal as the number of cycles reached 500 cycles as shown in Figs. 8 and 9. The observed images have shown that the cracks were mainly propagated near the surface without a penetration.

Usually a welded joint is known to be weaker than a base metal part. However, it is interesting to note that the crack propagation length for the base metal is larger than that of the filler metal as shown in Fig. 9. A few factors can be attributed to this finding. First, the creep rupture strength of the weld metal is higher than the base metal. Fig. 10 shows the minimum stress-to-rupture curve for 304 and 316 in ASME-NH (2004). The differences in the creep strength become more distinguished as the hold time increases. As the accumulated hold time is increased from 1, 10, 100 and 1,000 hours, the differences in the rupture

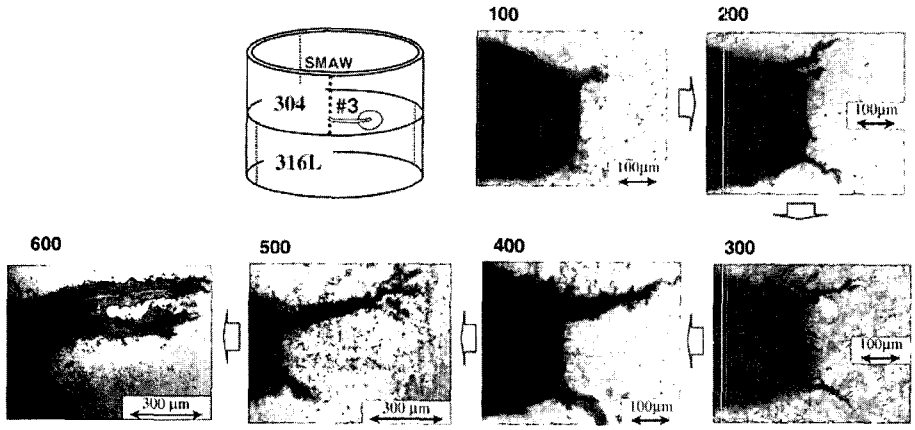

Fig. 8 Observed images at the horizontal defect #3 (base metal, 350×)

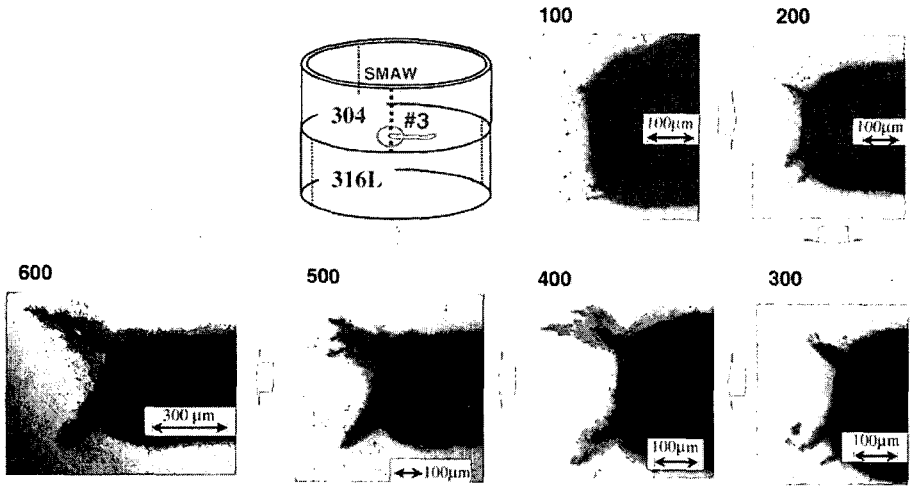

Fig. 9 Observed images at the horizontal defect #3 (weld metal, 350×)

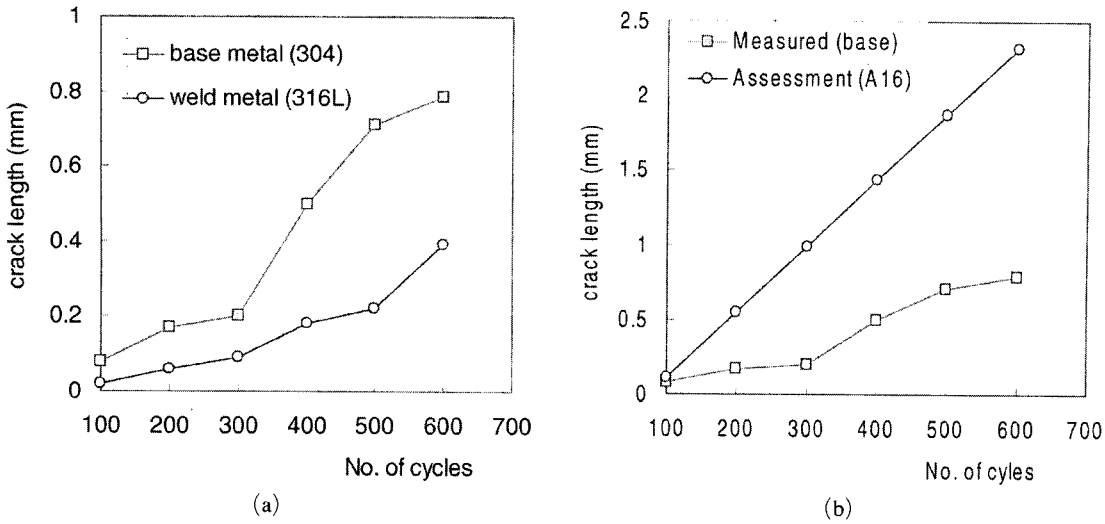

Fig. 10 Aspects of crack propagation observed at defect #3

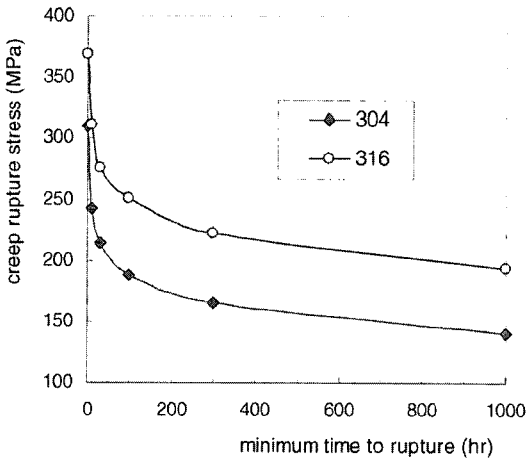

Fig. 11 Minimum stress-to-rupture curve

stress becomes 19%, 28%, 34% and 38% (ASME, 2004), respectively as shown in Fig. 11. Therefore, the main reason can be said to be caused by the differences of the creep rupture strength between the two materials. It should be noted that the defect has been machined at a weld metal part rather than a HAZ.

Second, the fracture toughness of the filler metal is higher than that of the base metal so that once a crack is initiated at both notches, a crack for the base metal would be propagated faster. The image of Fig. 9 observed at the weld line of 304-316L after 100 cycles shows that the 304 SS is weaker than the ER316L. And it should be noted that no internal or external weld defects near defect #3 were confirmed through the X-ray diffraction method before the test started. When the images are magnified, it was found that the micro-crack was propagating in the intergranular mode.

The yield strength of 304, 316L and the filler metal made of ER316L at room temperature is 274 MPa, 231 MPa and 258 MPa, respectively, which means that there is a strength under-match between 304 and the weld metal (ER316L) at defect #3. The strength data was measured by using a plate type material specimen sampled from the same structural material. It should be noted that the surface is usually hardened due to a cold working or a surface machining so that its strength on the surface is usually higher than the above values, and thus the fracture toughness would be slightly reduced.

The vertical defects of #2 and #6 have shown less damage than the horizontal defects as shown in Fig. 12 (magnification factor of 350, after 600 cycles). When comparing the two welding methods after finishing 600 load cycles, it was shown that the images by GTAW were slightly more damaged than that by SMAW. Since the mechanical stresses are acting in the axial direction, the damage at the vertical defects was less severe than that for the horizontal defects.

The images of surface defects #1 (SMAW) and #5 (GTAW) which were similar metal welds between the 316L and 316L steels shows that the damage for the GTAW was slightly more severe than that for the SMAW as shown in Fig. 13. From the above two observations on the vertical and surface defects, GTAW was shown to be weaker than SMAW at similar metal welds.

The observed images for defect #8 which is located along the dissimilar metal weld line of 304 and the 316L materials show that the damage for a GTAW is less severe than that for a SMAW as shown in Fig. 14. It is worth noting that defect #8 which was machined along the weld interface line is stronger than the base metal part of 304 SS at defect #3. In a dissimilar metal weld between 304 and 316L, the SMAW method was observed to be weaker to a creep-fatigue load than the GTAW method as shown in Figs. 14.

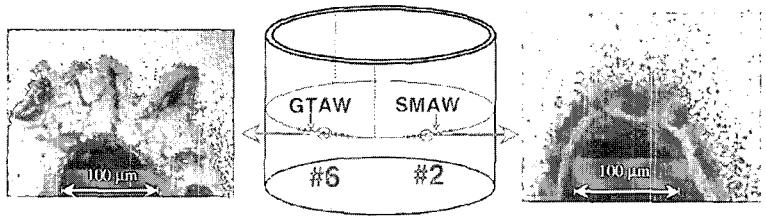

Fig. 12 Observed images of the surface defects (#2, #6 ; 600 cycles, 350×)

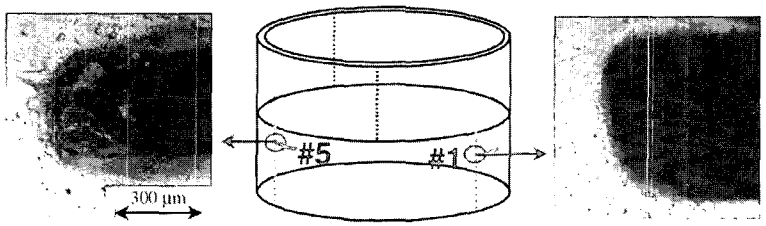

Fig. 13 Observed images of the surface defects (#1, #5 ; 600 cycles, 350×)

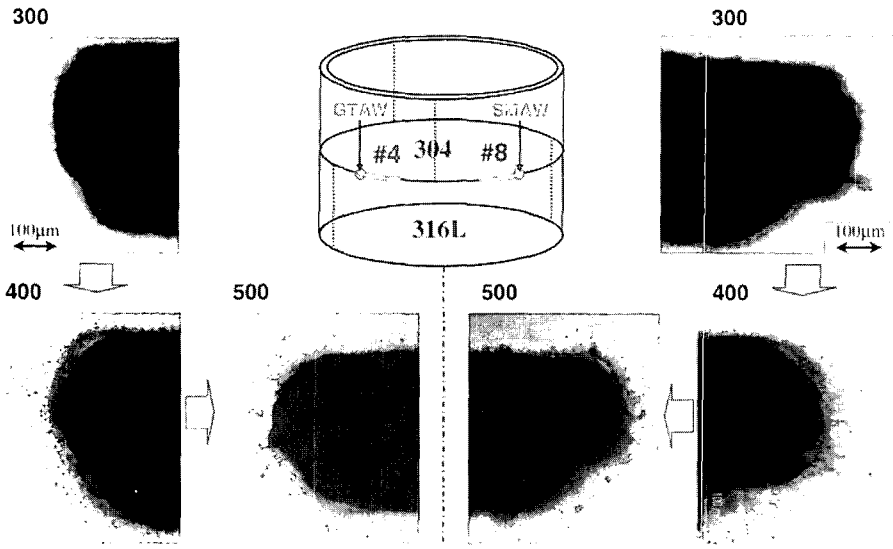

Fig. 14 Observed images of the horizontal defect #8, 350×)

5. Conclusions

A study on a creep-fatigue crack growth for a welded cylindrical shell has been carried out by using the structural test and evaluation according to the French assessment procedure of RCC-MR A16. The test specimen has the dimensions of a 600 mm outer diameter, a 500 mm height and a 7 mm thickness. The specimen is a welded cylindrical shell with one half a 304 SS shell and the other half 316L SS by using the welding methods of a SMAW and a GTAW. Eight defects were machined on or near the welded joints. One of the tips for each crack-like defect was machined to be located on the weld metal part rather than the heat affected zone.

The assessment of the creep-fatigue crack propagation for the base metal notch part at defect #3 according to A16 procedure showed that the increment of a fatigue crack growth per cycle was 0.00268 mm while that of a creep crack growth under one hour's hold time was 0.49 mm. As for the creep-fatigue crack propagation for the weld metal, the fatigue crack growth increment was 0.00225 mm and the creep crack growth increment was 0.23 mm. These assessment results according to the A16 guide show that A16 is overly conservative for a crack growth assessment in the case of a short hold time like one-hour of the present case. It is clear that a crack propagation is dominated by a creep crack growth. The crack propagation for the base metal was larger than that for the weld metal. This result is mainly attributed to the superior creep properties of the weld metal of ER316L to the base metal of 304.

The creep-fatigue damage was observed with a portable optical microscope intermittently at every 100^{th} cycle non-destructively. The observed images showed that the damage for the 304 SS base metal part was measured to be more severe than that of the weld metal (ER316L). The horizontal defects were weaker than the vertical defects because the primary stresses were acting axially. The amount of creep-fatigue crack propagation at the crack tip for the 304 SS base metal (defect #3) was measured to be 0.79 mm after 600 load cycles. The present creep-fatigue problem is creep dominant and a crack initiation and propagation occurred mainly due to a creep. The images of the damage at the tips of the notch showed that a crack propagation occurred in an intergranular cracking mode.

The behavior of the two welding methods of a SMAW and a GTAW under a creep-fatigue load was examined. From the creep-fatigue test up to 600 load cycles, the GTAW was observed to be weaker than SMAW at the similar metal weldments while SMAW was weaker than GTAW at the dissimilar metal welds.

When the results from the assessment according to the A16 procedure and structural test are compared, A16 seems to be overly conservative for a creep-fatigue crack propagation in the case of a short hold time like one hour of the present study.

Acknowledgments

This work was performed under the long term nuclear R&D program sponsored by the Ministry of Science and Technology of Korea.

References

A16, 2002, Subsection Z ; Technical Appendix A16 of RCC-MR, "Guide for Leak Before Break Analysis and Defect Assessment," AFCEN.

A3, 2002, Subsection Z : Technical Appendix A3, RCC-MR, AFCEN.

ABAQUS Users manual, 2005, Version 6.5, H. K.S, USA.

ASME Boiler and Pressure Vessel Code, 2004, Section III, Rules for Construction of Nuclear Power Plant Components, Div. 1, Subsection NH, Class 1 Components in Elevated Temperature Service.

British Energy Generation Ltd, 2001, *Assessment of the Integrity of Structures Containing Defects*, R6 Rev. 4. British Energy Generation Ltd, UK.

British Standard Institution, 2000, *Guide on Methods for Assessing the Acceptability of Flaws in Metallic Structures*, BS7910 : 1999 (Rev. March 2000) British Standards Institution, London, UK.

Chellapandi, P., Chetal, S. C. m Raj, Baldev., 2005, "Assessment of σ_d Approach for Creep Damage Estimation of FBR Components With Crack Like Defects at Welds," *IJPVP*, Vol. 82, pp. 739~745.

DDS, 1998, Structural Design Guide for Class 1 Components of Prototype Fast Breeder Reactor for Elevated Temperature Service, JAPC, Japan.

Drubay, B., Marie, S., Chpuliot. S., Lacire, M. H., Michel, B. and Deschanels, H., 2003, "A16 : Guide for Defect Assessment at Elevated Temperature," *International Journal of Pressure Vessel and Piping*, Vol. 80, pp. 499~516.

Hahn, D. -H. et al., 2004, *KALIMER Preliminary Conceptual Design Report*, KAERI/TR-2204, Korea Atomic Energy Research Institute, Daejeon.

Kim, J. B., Park, C. -G., Lee, H. -Y. and Lee, J. -H., 2005, *Experiment and Analysis on the Creep-fatigue Damage of 316 SS nonlinear Structure in Liquid Metal Reactor Subjected to Cyclic Loading with 1hr Hold Time*, 18th Int. Conf. on Structural Mechanics in Reactor Technology, Beijing, China, August 7.

Kraus, H., Creep Analysis, 1980, John Wiley & Sons.

Lee, H. -Y and Nikbin, K. M., 2006d, "Modelling the Redistribution of Residual Stresses at Elevated Temperature in Components," *Journal of ASTM International*, Vol. 3(1), pp. 1-15.

Lee, H. -Y., Biglari, F., Wimpory, R., O'Dowd, N. P., Nikbin, K. M., 2006b, "Treatment of Residual Stresses in Life Assessment Procedures," *Engineering Fracture Mechanics*, Vol. 73, pp. 1755~1771.

Lee, H. -Y., Kim, J. -B., Kim, S. -H. and Lee, J. -H, 2006a, "Assessment of Creep-Fatigue Crack Initiation for Welded Cylindrical Structure of Austenitic Stainless Steels," *International Journal of Pressure Vessel and Piping*, in press, April.

Lee, H. -Y., Kim, J. -B. and Lee, J. -H., 2004, "Evaluation of Progressive Inelastic Deformation for the Welded Structure Induced by Spatial Variation of Temperature," *International Journal of Pressure Vessel and Piping*, Vol. 81(5), pp. 433~441.

Lee, H. -Y., Kim, J. -B. and Lee, J. -H., 2003, "Progressive Inelastic Deformation Characteristics of Cylindrical Structure with Plate-to-shell Junction Under Moving Temperature Front," *Korean Society of Mechanical Engineering International Journal*, Vol. 17(3), pp. 403~411.

Lee, H. -Y., Kim, J. -B. Lee, J. -H. and Nikbin, K. M., 2006c, "Comprehensive Residual Stress Distribution for a Plate and Pipe Components," *Journal of Mechanical Science and Technology*, Vol. 20, No. 3, pp. 335~344.

RCC-MR, 2002, Design and Construction Rules for Mechanical Components of FBR Nuclear Islands, Edition 2002, AFCEN.